Photonics and Nanostructures - Fundamentals and Applications 32 (2018) 19–23

Contents lists available at ScienceDirect

Photonics and Nanostructures - Fundamentals and Applications

journal homepage: www.elsevier.com/locate/photonics

Particle swarm optimized ultra-compact polarization beam splitter on silicon-on-insulator

Qichao Lu[a], Wei Wei[b,*], Xin Yan[a], Bing Shen[c], Yanbin Luo[a], Xia Zhang[a,*], Xiaomin Ren[a]

[a] State Key Laboratory of Information Photonics and Optical Communications, Beijing University of Posts and Telecommunications, Beijing, 100876, China
[b] School of Mechanical and Electric Engineering, Guangzhou University, Guangzhou, 510006, China
[c] 4catalyzer Inc., Guilford, 06437, USA

ARTICLE INFO

Keywords:
Particle swarm optimized
Inverse design
High extinction ratio
Tolerance

ABSTRACT

We have designed an ultra-compact polarization beam splitter on silicon-on-insulator (SOI). The device is designed by a Particle swarm optimized (PSO) inverse-design method with a quite small footprint of $2 \times 2\,\mu m^2$. Simulation results shows that the transmission is 61% for TE mode and 52% for TM mode at designed wavelength 1550 nm. The extinction ratio of our device is greater than 10dB within a bandwidth of 40 nm (1528–1567 nm). Benefiting from the global optimization of our inverse-design method, the transmission and extinction ratio can keep greater than 40% and 10 dB separately for both polarizations when the designed pixel side length varies from 100 to 130 nm. Besides, we demonstrate that the design method could have tolerance for input waveguide width, in this case, the device could maintain functionality while the width of input waveguide ranges from 300 to 350 nm.

1. Introduction

Recently, photonic-integrated circuits (PICs) fabricated on the silicon-on-insulator (SOI) platform have attracted substantial attention due to the low power consumption, high transmit efficiency, small footprint, as well as the compatibility with complementary metal-oxide-semiconductor (CMOS) fabrication process [1–5]. The high refractive index contrast of SOI permits sharp waveguide bends and ultra-small device sizes allowing for such high density integration. However, the high refractive index contrast results in strong birefringence, leading to polarization-sensitive performance, which has bad influence on photonic integrated circuits (PICs). Because polarization states can change randomly in optical fibers, the polarization sensitivity is a problem for compatibility between on-chip PICs and optical fibers [6]. Therefore, the polarization control in the process of optical transmission in PICs is essential. In PICs, the polarization beamsplitter (PBS), which splits or combines the orthogonal TE and TM modes, is a fundamental component for polarization control. In consequence, a PBS compact in size, easy to fabricate and low loss should be designed to fit the require of PICs.

Various kinds of waveguide-type PBSs have been reported such as multimode interference (MMI) structures [7–9], Mach–Zehnder interferometers [10–12], and directional couplers(DCs) [13–20] based PBSs. Among them, smaller footprint PBS devices who could be integrated are preferred. Therefore, different methods are used to decrease the size of PBSs on PIC. In 2013, a DC-based PBS composed of a hybrid plasmonic waveguide and a silicon nanowire was reported by Guan and colleagues [21]. Their device has dimensions of $1.9 \times 3.7 = 7.03\ \mu m^2$, but the incorporation of metal creates significant parasitic absorption losses and renders the process complementary metal–oxide–semiconductor (CMOS) incompatible. While in 2015, B Shen and his colleagues proposed a free-form metamaterial based PBS with an ultra-small footprint $2.4 \times 2.4 = 5.76\,\mu m^2$ [22]. The free-form metamaterial based PBS has a small footprint and is CMOS compatible, but the device size could still be decreased.

In contrast to previous device designs, we demonstrate the use of an inverse design method that explores the full design space and allows us to design devices with previously unattainable functionality, higher performance and robustness, and smaller footprints than conventional devices [23]. Previously in [23], an alternating directions method of multipliers (ADMM) algorithm was used to optimize the inverse design method. Their optical simulation was based on a home-built finite-difference frequency-domain (FDFD) solver. Various ultra-compact devices including, sub-wavelength optical gratings [24], wavelength de-multiplexing grating coupler [25], and wavelength splitters [26] were created by the ADMM based method. Here we proposed a Particle swarm optimized (PSO) algorithm based inverse design method. The optical simulation was supported by a finite-difference time-domain

* Corresponding authors.
E-mail addresses: wei@gzhu.edu.cn (W. Wei), xzhang@bupt.edu.cn (X. Zhang).

https://doi.org/10.1016/j.photonics.2018.08.006
Received 15 July 2018; Received in revised form 31 August 2018; Accepted 31 August 2018
Available online 05 September 2018

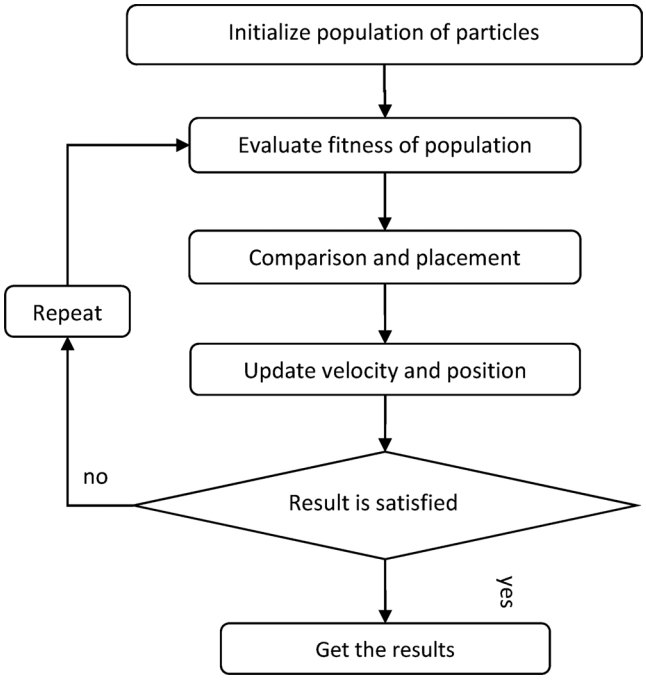

Fig. 1. Flow chart of PSO algorithm.

(FDTD) solver. Our method allows the user to 'design by function', whereby the user could simply specify the desired functionality of the device, and the algorithm finds a structure that meets these requirements. In particular, our algorithm searches the full design space of devices with arbitrary topologies. Moreover, the convergence speed of our method is controllable to increase the computing efficiency. Due to the greatly expanded design space, the complex and aperiodic structure can provide previously unattainable functionality, higher performance or smaller footprints than traditional devices.

In general, we use a computationally inverse design to engineer the refractive index of a region of silicon to achieve a specific photonic function. In our case, the function is polarization beam splitter in a waveguide. Here, we have designed and characterized an ultra-compact PBS with a footprint of only $2 \times 2 = 4\,\mu m^2$ for a designed wavelength of 1550 nm in simulation. The PBS is patterned on an SOI substrate, in which the thicknesses of the silicon is 300 nm. The PBS is comprised of only silicon which is CMOS compatible and can be fabricated with a single lithography step [27]. The transmission efficiencies for TE and TM modes at 1550 nm are 61% and 52%, respectively. The operation bandwidth of the PBS, defined as the range extinction ratio greater than 10 dB, is 40 nm (1528–1567 nm). Since the inverse design method allows the geometry of the device to be freely optimized, our device not only exhibit a small footprint, but are also expected to be fairly tolerant to fabrication errors. Besides, our PBS could fit varied input waveguide of different width.

2. Design and simulation

Particle swarm optimization (PSO) was firstly proposed by Eberhart et al. through simulating the social behavior of flying birds [28]. Each individual, called a particle, adjusts its flight according to both its own and neighbor' flying experiences. The position of a particle is updated via the following equation,

$$x_{i,d} = x_{i,d} + \Delta t \tag{1}$$

$$v_{i,d} = \varpi_n \times v_{i,d} + c_1 \times rand() \times (p_{i,d} - x_{i,d}) + c_2 \times rand() \times (g_{i,d} - x_{i,d}) \tag{2}$$

Where $x_{i,d}$ is the ith particle's position in the dth dimension of the parameter space, and $v_{i,d}$ is the corresponding velocity. w_n is the inertial weight for nth iteration and determines how likely the particle stays on its old velocity. $p_{i,d}$ and $g_{i,d}$ are individual and global best positions, respectively. c_1 and c_2 are two positive constants, which determine how much a particle is influenced by the memory of its own best position and the global best position, respectively. In our case, a large inertial weight is used to traverse most of the design space and finally a smaller inertial weight is employed for convergence. The flow chart of PSO algorithm is shown in Fig. 1.

In this work, the objective of PSO is to obtain a design that splits a combined TE + TM signal transmitted from the input waveguide to two separate TE and TM modes. The design district is a square consisted of 20 × 20 pixels. Every pixel is in the shape of a square made of silicon or air with side length of 100 nm. Each pixel has two states "0″ and "1″, indicating the pixel's material: "0″ for air and "1″ for silicon. The pixels are seen as particles with identical states (instead of position) and velocity. A random initial state and velocity would be given to the particles, fitness for both single particle and the whole population would be calculated to find a best state during each iteration. The fitness in this

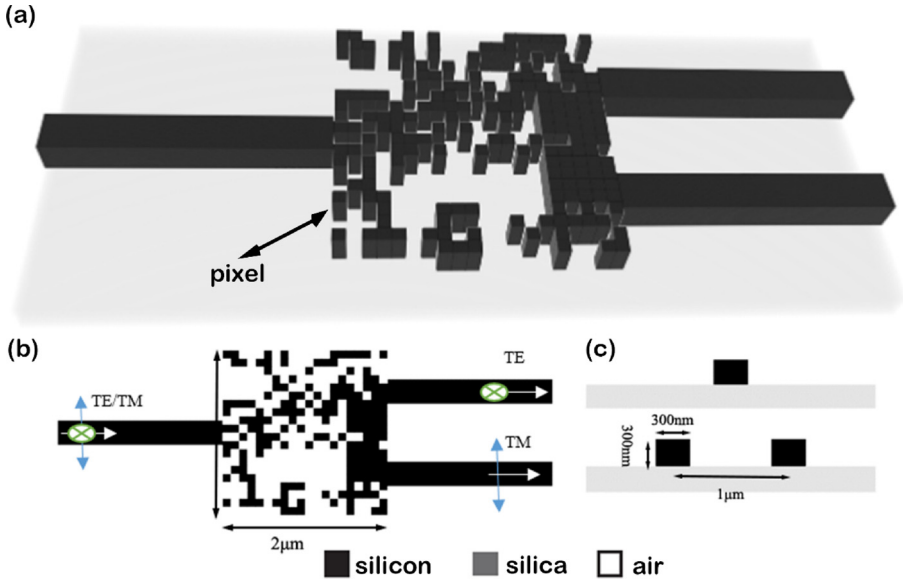

Fig. 2. Schematic diagram of the designed device. (a)3-d image of the device; cross section of the device from (b) up and (c) front and back sides.

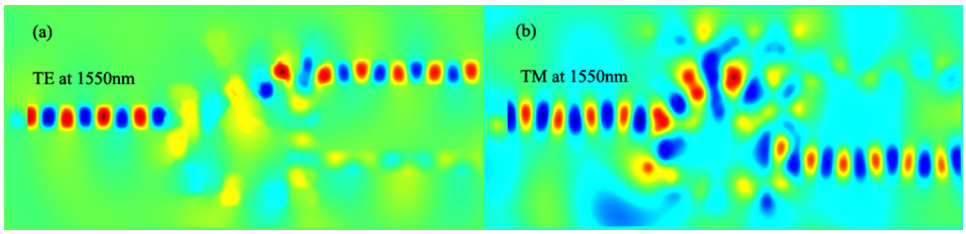

Fig. 3. Simulated steady-state intensity distributions for TE (a) and TM (b) polarized light at the wavelength of 1550 nm.

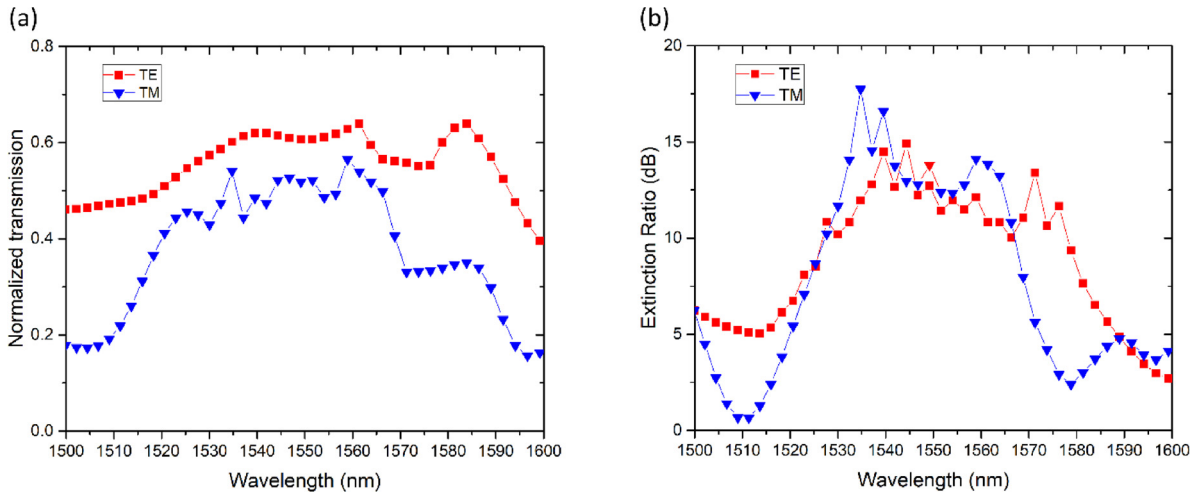

Fig. 4. Simulated performance of the PBS. (a) Simulated transmission efficiencies and (b) extinction ratios of the PBS for both TE (square) and TM (triangle) polarization.

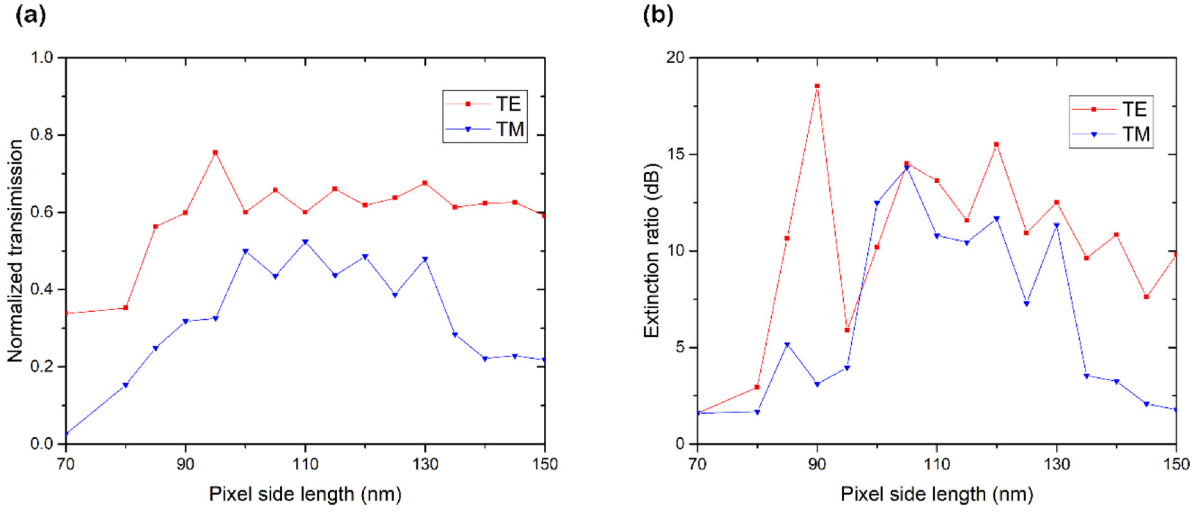

Fig. 5. (a) simulated transmission efficiencies and (b) extinction ratios as a function of pixel side length.

work is set as the average extinction ratio of the device from 1520 to 1565 nm. The iteration would stop if the fitness is satisfied or the preset iteration number is reached. Therefore, pixels seen as particles could finally find their states to get the best design of the device. The optimized device structure shown in Fig. 2 (a), consisting of a 2 μm × 2 μm rectangular region with a single-mode input waveguide supporting the TE and TM modes. The TE signal is designed to be transported to the upper output waveguide, while the TM signal is designed to be transported to the lower waveguide, as shown in Fig. 2 (b).

To study the performance of this PBS, a 3D-FDTD method is employed [29], formulas of which are directly derived from Maxwell's equations with the help of 3-D Yee's mesh. Meanwhile, perfect match layers (PMLs) are also imposed at the edges of the computational window. Through this method, the light field at the input and output ports can be obtained, which can be used to assess the performance of the device. The silicon device layer with a permittivity of $\varepsilon_{Si} = 11.97$ (refractive index 3.46) [30] is placed on top of a silica buffer layer with a permittivity of $\varepsilon_{silica} = 2.10$ (refractive index 1.45) [31]. At the far end of the input waveguide (Fig. 2 (b)), a gaussian plane wave is set as the light source. The up side cross section of device is shown in Fig. 2 (b), Fig. 2 (c) illustrates the front and back sides cross section of the device and marks the parameters of the input and output waveguides. Fig. 3 shows the simulated intensity distributions for both polarizations at 1550 nm. TE mode transported to the upper waveguide is shown in Fig. 3 (a), while Fig. 3 (b) illustrates the filed pattern of TM mode, respectively. It can be clearly seen that the beam splitting function works well at the designed wavelength 1550 nm.

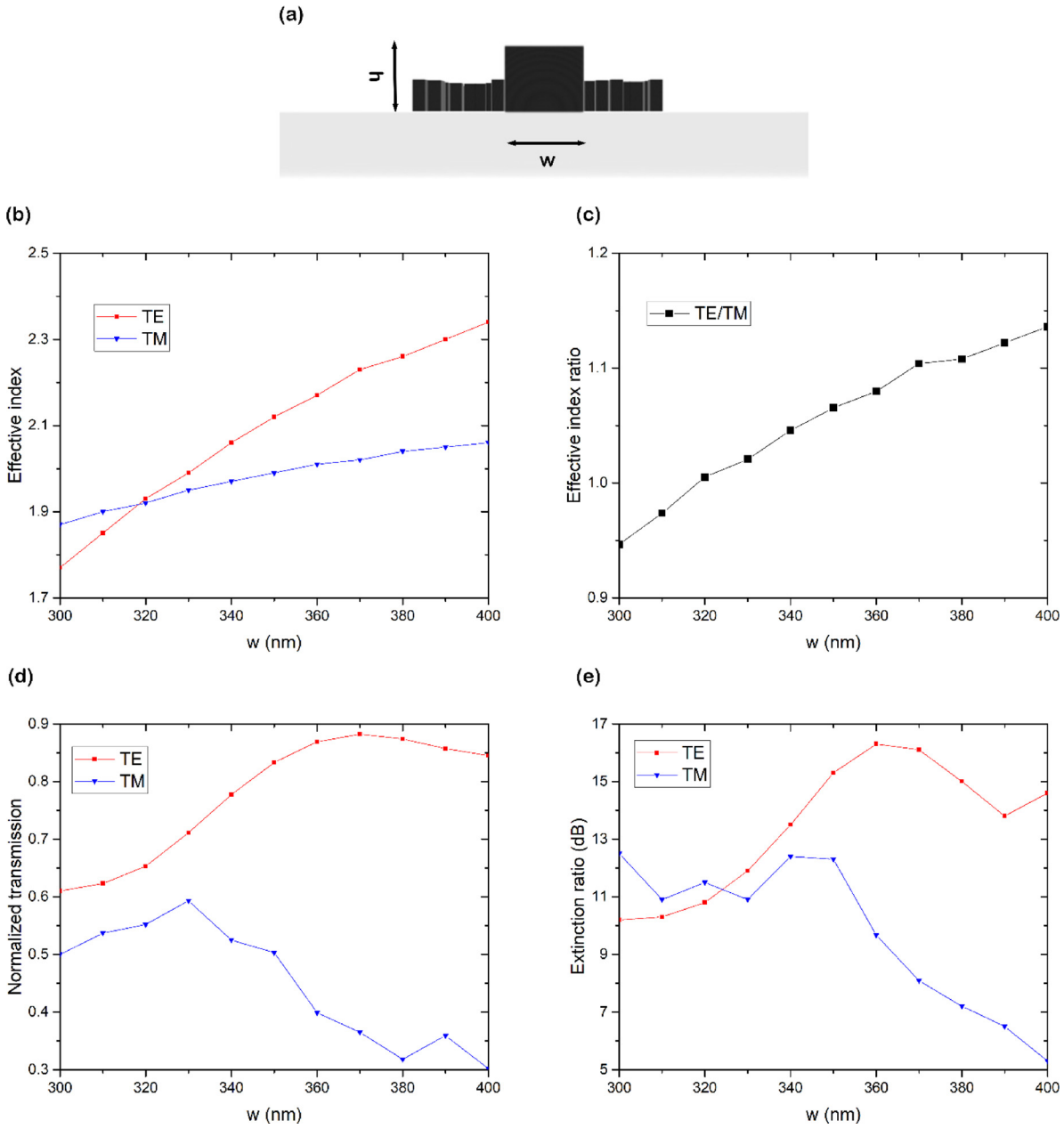

Fig. 6. (a) front side view of the input waveguide; (b) Effective mode indices of the Si waveguide for h = 300 nm, (c) TE and TM indices ratio, (d) simulated transmission efficiencies and (e) extinction ratios as a function of silicon waveguide width (w).

3. Results and discuss

We calculate and analyse the transmission efficiency and extinction ratio (ER) of this PBS. The wavelength-dependence transmission efficiency and ER of the PBS are illustrated in Fig. 4. The ERs at the upper and lower ports are defined as follows,

$$ER_{TE} = 10\log_{10}\frac{P_{TE,upper}}{P_{TE,lower}} \tag{3}$$

$$ER_{TM} = 10\log_{10}\frac{P_{TM,lower}}{P_{TM,upper}} \tag{4}$$

where $P_{TE,upper}$ and $P_{TE,\mathrm{lower}}$ are the output powers for the TE mode at the upper port and lower port, while $P_{TM,upper}$ and $P_{TM,\mathrm{lower}}$ represent the transmittances from the upper and lower ports for the TM mode, respectively.

Coupling efficiencies of 61% and 52% are obtained at the designed wavelength (1550 nm) for TE and TM. The efficiency is not as high as previous PBS in Ref [22]. Therefore, we have considered some ways to increase the efficiency of our device in the future. One way is to increase the calculation accuracy, expand the search space of our algorithm. The other way is to change the shape of our “pixels”, the devices with pixels of different shapes display different scatter fields. We assume that the device could have better performance using a design with other shape pixels. Fig. 4 (a) shows that the transmission of TE mode keeps steady in a relatively broader range while the transmission of TM mode decreases fast when wavelength < 1530 nm or > 1555 nm. We assume that TE mode are widely existed in the SOI devices while the inverse designed ultra-compact device has wavelength selection effect for TM mode.

The measured TE and TM extinction ratios are 12.1 dB and 13.1 dB, respectively. The operational bandwidth of our device, in which the ERs at the upper and lower ports are more than 10 dB, is over the wavelength range of 1528–1567 nm (Fig. 4 (b)). The ERs of our device are

comparable to other device, while the operation bandwidth is relatively narrow. We assume that the polarization selection effect cumulated by a number of guided-mode resonances in small size device could be the reason [32]. Also, it can be clearly seen from Fig. 4(b) that the ERs for both TE and TM decrease rapidly while wavelength $>$ 1570 nm or $<$ 1525 nm. The reason might be that the smaller-size devices are more sensitive to wavelength [33]. However, respect to the ultra-small size of our device and C-band is covered in our operation bandwidth, the performance is acceptable.

The impact of the variation of the pixel side length on the device performance is simulated to elucidate the tolerance of small changes in the device geometry. The results for transmission efficiency and extinction ratio are illustrated in Fig. 5 (a), (b), respectively. It can be clearly seen that our device can remain functional while the pixel side length varies from 100 to 130 nm. Apparently, the device performance decreases rapidly when the pixel side length is $<$ 100 nm for both modes. We consider that the 100-nm-side-long pixel might be the limit of our method since it is rather difficult for modes to transport in such a small pixel.

The impact of the variation of the input waveguide width on the device performance is also simulated. Fig. 6 (a) shows the side view of the silicon waveguide, with a fixed height h (h = 300 nm) and width w. The TE and TM dependence of the effective indices on w is shown in Fig. 6 (b), while Fig.6 (c) show the effective indices ratio between the TE and TM mode. The quantity n_{TE} and n_{TM} monolithically increases with the increase of the waveguide width. The results of the transmission efficiency and extinction ratio are illustrated in Fig. 6 (c) and (d), respectively. For extinction ratio is greater than 10 dB, the devices can fit different input silicon waveguide whose width varies from 300 to 350 nm. The transmission and extinction ration for TM mode decrease rapidly when w $>$ 350 nm whereas the effective indices between two modes have little difference. The reason may be that the TM mode in wider Si waveguide becomes weaker and couples less while TE mode do not [34,35].

From both the analysis results of pixel side length and input waveguide width, it is well illustrated that the device performance for TM mode is the key point for the design of PBS. Therefore, in our future work the TM mode should be considered more to design device with more outstanding performance.

4. Conclusions

We have demonstrated the utilization of PSO for the design of a PBS for the fundamental TE and TM modes, which has a rather small footprint ever of 2 μm × 2 μm. It is an ultra-compact device without a loss of the general functionality. The extinction ratio was measured to be more than 10 dB in a bandwidth of 40 nm. In addition, the PBS also has a relatively large tolerance for pixel size. Benefiting from the inverse-design method, the transmission and extinction ratio can be kept functional for both polarizations when the designed pixel side length varies from 100 to 130 nm. Besides, our device could fit input waveguide whose width ranges from 300 to 350 nm without function loss. We believe that the performance can be improved through further optimizations, but here we have demonstrated that the technique can be expanded to include more functions. Therefore, the PSO method could be employed to create ultra-compact devices such as mode splitter and multiplexer required for photonic integrated components in the future.

Acknowledgements

This work was supportedby the National Natural Science Foundation of China (61774021 and 61504010), and the Fund of State Key Laboratory of Information Photonics and Optical Communications (Beijing University of Posts and Telecommunications), P. R. China (IPOC2017ZT02).

References

[1] D. Liang, J.E. Bowers, Recent progress in lasers on silicon, Nat. Photonics 4 (8) (2010) 511.
[2] G.T. Reed, G. Mashanovich, F.Y. Gardes, et al., Silicon optical modulators, Nat. Photonics 4 (8) (2010) 518.
[3] R. Nagarajan, C.H. Joyner, R.P.J. Schneider, J.S. Bostak, T. Butrie, A.G. Dentai, V.G. Dominic, P.W. Evans, M. Kato, M. Kauffman, et al., Large-scale photonic integrated circuits, Ieee J. Sel. Top. Quantum Electron. 11 (2005) 50–65.
[4] V.R. Almeida, C.A. Barrios, R.R. Panepucci, et al., All-optical control of light on a silicon chip, Nature 431 (7012) (2004) 1081.
[5] C. Manolatou, et al., High density integrated optics, J. Lightwave Technol. 17 (1999) 1682–1692.
[6] T. Barwicz, M.R. Watts, M.A. Popović, et al., Polarization-transparent microphotonic devices in the strong confinement limit, Nat. Photonics 1 (1) (2007) 57.
[7] B.K. Yang, S.Y. Shin, D. Zhang, Ultrashort polarization splitter using two-mode interference in silicon photonic wires, Ieee Photonics Technol. Lett. 21 (7) (2009) 432–434.
[8] A. Hosseini, S. Rahimi, X. Xu, et al., Ultracompact and fabrication-tolerant integrated polarization splitter, Opt. Lett. 36 (20) (2011) 4047–4049.
[9] M. Yin, W. Yang, Y. Li, et al., CMOS-compatible and fabrication-tolerant MMI-based polarization beam splitter, Opt. Commun. 335 (2015) 48–52.
[10] T.K. Liang, H.K. Tsang, Integrated polarization beam splitter in high index contrast silicon-on-insulator waveguides, Ieee Photonics Technol. Lett. 17 (2) (2005) 393–395.
[11] D. Dai, Z. Wang, J. Peters, et al., Compact polarization beam splitter using an asymmetrical Mach–Zehnder interferometer based on silicon-on-insulator waveguides, IEEE Photonics Technol. Lett. 24 (8) (2012) 673–675.
[12] D. Pérez-Galacho, R. Halir, A. Ortega-Moñux, et al., Integrated polarization beam splitter with relaxed fabrication tolerances, Opt. Express 21 (12) (2013) 14146–14151.
[13] N.C. Cheng, Y.F. Ma, P.H. Fu, et al., Horizontal slot waveguides for polarization branching control, Appl. Opt. 54 (3) (2015) 436–443.
[14] B. Chen, C. Liu, G. Liu, Study on compact polarization beam splitters based on directional coupling in Bragg reflection waveguides, Appl. Opt. 54 (12) (2015) 3624–3629.
[15] D. Dai, Z. Wang, J.E. Bowers, Ultrashort broadband polarization beam splitter based on an asymmetrical directional coupler, Opt. Lett. 36 (13) (2011) 2590–2592.
[16] D. Dai, Silicon polarization beam splitter based on an asymmetrical evanescent coupling system with three optical waveguides, J. Light. Technol. 30 (20) (2012) 3281–3287.
[17] D. Dai, J.E. Bowers, Novel ultra-short and ultra-broadband polarization beam splitter based on a bent directional coupler, Opt. Express 19 (19) (2011) 18614–18620.
[18] J. Wang, J. Xiao, X. Sun, Design of a compact polarization splitter composed of a multiple-slotted waveguide and a silicon nanowire, J. Opt. 15 (3) (2013) 035501.
[19] Z. Ying, G. Wang, X. Zhang, et al., Ultracompact and broadband polarization beam splitter based on polarization-dependent critical guiding condition, Opt. Lett. 40 (9) (2015) 2134–2137.
[20] Y. Xu, J. Xiao, Design of a compact and integrated TM-rotated/TE-through polarization beam splitter for silicon-based slot waveguides, Appl. Opt. 55 (3) (2016) 611–618.
[21] X. Guan, H. Wu, Y. Shi, et al., Ultracompact and broadband polarization beam splitter utilizing the evanescent coupling between a hybrid plasmonic waveguide and a silicon nanowire, Opt. Lett. 38 (16) (2013) 3005–3008.
[22] B. Shen, P. Wang, R. Polson, et al., An integrated-nanophotonics polarization beamsplitter with 2.4× 2.4 μm 2 footprint, Nat. Photonics 9 (6) (2015) 378.
[23] J. Lu, J. Vučković, Nanophotonic computational design, Opt. Express 21 (11) (2013) 13351–13367.
[24] A.C.R. Niederberger, D.A. Fattal, N.R. Gauger, et al., Sensitivity analysis and optimization of sub-wavelength optical gratings using adjoints, Opt. Express 22 (11) (2014) 12971–12981.
[25] A.Y. Piggott, et al., Inverse design and implementation of a wavelength demultiplexing grating coupler, Sci. Rep. 4 (2014).
[26] A.Y. Piggott, J. Lu, K.G. Lagoudakis, et al., Inverse design and demonstration of a compact and broadband on-chip wavelength demultiplexer, Nat. Photonics 9 (6) (2015) 374–377.
[27] T.K. Liang, H.K. Tsang, Integrated polarization beam splitter in high index contrast silicon-on-insulator waveguides, Ieee Photonics Technol. Lett. 17 (2) (2005) 0393–0395.
[28] R. Eberhart, J. Kennedy, A new optimizer using particle swarm theory, In MHS'95. Proceedings of the Sixth International Symposium on Micro Machine and Human Science, (IEEE), (2018), pp. 39–43.
[29] A.F. Oskooi, D. Roundy, M. Ibanescu, et al., MEEP: A flexible free-software package for electromagnetic simulations by the FDTD method, Comput. Phys. Commun. 181 (3) (2010) 687–702.
[30] H.H. Li, Refractive index of silicon and germanium and its wavelength and temperature derivatives, J. Phys. Chem. Ref. Data 9 (3) (1980) 561–658.
[31] I.H. Malitson, Interspecimen comparison of the refractive index of fused silica, Josa 55 (10) (1965) 1205–1209.
[32] A. Valle, L. Pesquera, K.A. Shore, Polarization selection and sensitivity of external cavity vertical-cavity surface-emitting laser diodes, Ieee Photonics Technol. Lett. 10 (5) (1998) 639–641.
[33] Q. Xu, B. Schmidt, J. Shakya, et al., Cascaded silicon micro-ring modulators for WDM optical interconnection, Opt. Express 14 (20) (2006) 9431–9436.
[34] C.W. Hsu, T.K. Chang, J.Y. Chen, et al., 8.13 μm in length and CMOS compatible polarization beam splitter based on an asymmetrical directional coupler, Appl. Opt. 55 (12) (2016) 3313–3318.
[35] Y. Zhang, Y. He, J. Wu, et al., High-extinction-ratio silicon polarization beam splitter with tolerance to waveguide width and coupling length variations, Opt. Express 24 (6) (2016) 6586–6593.